




Renormalization of the shell model of turbulence

Mahendra K. Verma ^{1,*} and Shadab Alam ^{2,†}

¹*Department of Physics, Indian Institute of Technology Kanpur, Kanpur 208016, India*

²*Department of Mechanical Engineering, Indian Institute of Technology Kanpur, Kanpur 208016, India*

 (Received 26 November 2022; revised 7 April 2023; accepted 17 May 2023; published 20 June 2023)

Renormalization enables a systematic scale-by-scale analysis of multiscale systems. In this paper, we employ *renormalization group* (RG) to the shell model of turbulence and show that the RG equation is satisfied by $|u_n|^2 = K_{\text{Ko}} \epsilon^{2/3} k_n^{-2/3}$, where Ko is the Kolmogorov constant and $v_n = v_* \sqrt{K_{\text{Ko}}} \epsilon^{1/3} k_n^{-4/3}$, where k_n and u_n are the wave number and velocity of shell n ; v_* and K_{Ko} are RG and Kolmogorov's constants; and ϵ is the energy dissipation rate. We find that $v_* \approx 0.5$ and $K_{\text{Ko}} \approx 1.7$, consistent with earlier RG works on the Navier-Stokes equation. We verify the theoretical predictions using numerical simulations.

DOI: [10.1103/PhysRevE.107.064118](https://doi.org/10.1103/PhysRevE.107.064118)

I. INTRODUCTION

Renormalization group (RG) analysis has been employed to model turbulence. Orszag [1] and Forster *et al.* [2] performed one of the first perturbative renormalization analysis. Yakhot and Orszag [3] performed detailed analysis using ϵ expansion. The other perturbative RG works are by Zhou *et al.* [4], Zhou [5], McComb and Shanmugasundaram [6,7], McComb [8,9], Eyink [10], Martin *et al.* [11], Bhattacharjee [12], and Adzhemyan *et al.* [13]. Among these works, McComb, Zhou, and coworkers employed self-consistent RG (using the “dressed Green’s function”) that has nonperturbative features. The above set of works show that the renormalized turbulent viscosity $\nu(k) \sim k^{-4/3}$, where k is the wave number.

Recently, researchers have employed *exact renormalization group equation* (ERGE) to turbulence [14–16]. Here, either sharp or smooth filter is employed during coarsening. A more formal implementation of ERGE is via functional renormalization group (FRG). Tomassini [17], Fontaine *et al.* [18], and Canet [19] employed FRG to hydrodynamic turbulence and the shell model. They derived formulas for the velocity correlations and multiscaling exponents. For the Navier-Stokes equation (NSE), Canet [19] reported $\nu(k) \approx k^{-1}$, rather than $\nu(k) \sim k^{-4/3}$. Fedorenko *et al.* [20] performed FRG to decaying Burgers, hydrodynamic, and quasigeostrophic turbulence. Among many results, Fedorenko *et al.* [20] showed that for hydrodynamic turbulence, the second-order structure function scales as l (the distance between two points), rather than Kolmogorov’s predictions of $l^{2/3}$.

Mejía-Monasterio and Muratore-Ginanneschi [21] performed nonperturbative renormalization group analysis of stochastic Navier-Stokes equation with power-law forcing. Here, they renormalized the viscosity, the forcing amplitude, and the coupling constants. Using field-theoretic tools,

Biferale *et al.* [22] constructed optimal subgrid closure for the shell models; they related the closure scheme to *large-eddy simulations*. In addition, Eyink [10] used *operator product expansion* and discovered *multiscaling* for the shell model. Some other notable field-theoretic works (not RG) on turbulence are Refs. [23–26].

In this paper, we employ the RG scheme based on the differential equation as in Refs. [3,4,8]. Note that the shell model involves discrete wave numbers, hence, its renormalization does not involve complex integration as in hydrodynamic turbulence. For the inviscid shell model, our RG procedure yields $\nu(k) = 0$ as the solution of the RG equation, which is similar to the Gaussian fixed point of Wilson ϕ^4 theory [27]. We verify several RG predictions using numerical simulation of the shell model. We use temporal autocorrelation function for the velocity field to compute the renormalized viscosity [28,29].

In one of the important works on hydrodynamic turbulence, Kraichnan [30] argued that large-scale structures sweep the small-scale fluctuations; this phenomenon is referred to as the *sweeping effect*. These interactions are naturally multiscale (across many wave numbers). Note, however, that multiscale interactions are absent in the shell models, which has local interactions among the wave number shells. Hence, we expect that sweeping effect may be suppressed in the shell model. This is precisely what we observe in our RG calculation of the shell model.

In this paper, we compute the renormalized viscosity in the shell model using momentum-space RG proposed by Wilson and Kogut [27] (see Sec. II). Here, we assume that the coarse-grained velocity field is random satisfying time stationarity. Our calculation does not require quasi-Gaussian approximation for the velocity field. In Sec. III, we compute the energy flux of the shell model; here, we assume the velocity field to be quasi-Gaussian. The flux calculation enables us to compute Kolmogorov’s constant. Interestingly, our predictions for the shell model are quite close to those for the Navier-Stokes equation. In Sec. IV, we extend our RG calculation to show that sweeping effect is suppressed in the shell model.

*mkv@iitk.ac.in

†shadab@iitk.ac.in

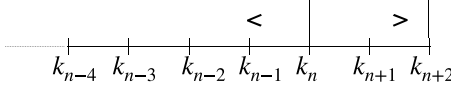


FIG. 1. Division of wave number shells into $>$ and $<$ partitions during the computation of v_n at $k = k_n$. Under the coarse graining, the $u^<$ variables are unaltered, whereas $u^>$ variables are averaged out.

In Sec. V, we describe how we verify the theoretical predictions using numerical simulations. We observe that the numerical results are in good agreement with the theoretical predictions. In Sec. VI, we compare our results with those from earlier works. We conclude in Sec. VII.

II. RENORMALIZATION OF VISCOSITY

The Sabra shell model is [31–36]

$$\frac{du_n}{dt} + \bar{\nu}k_n^2 u_n = -i\lambda [a_1 k_n u_{n+1}^* u_{n+2} + a_2 k_{n-1} u_{n-1}^* u_{n+1} - a_3 k_{n-2} u_{n-1} u_{n-2}] + f_n, \quad (1)$$

where u_n represents the velocity field for the shell n ; $\bar{\nu}$ is the *microscopic kinematic viscosity*; a_1, a_2 , and a_3 are constants with $a_1 + a_2 + a_3 = 0$; and $k_n = k_0 b^n$ with b as a constant. In this paper, we choose $a_1 = 1, a_2 = -1 + 1/b, a_3 = -1/b$, and b in the range of $(1.2, 2)$. Here, f_n represents the forcing, which is employed at small n 's. This forcing injects energy at large scales that cascades to small scales as the energy flux. Note that triadic interactions of hydrodynamic turbulence are modeled better with the Sabra model than the GOY model [31].

The coupling constant (coefficient of the nonlinear term) λ is not renormalized due to the Galilean invariance [2,9,37], and we set $\lambda = 1$. Refer to Appendix A for details. In addition, we consider u_n to be random as in fully developed turbulence, rather than introducing a separate noise term in the inertial range [5,6,37,38]. Thus, we avoid noise renormalization. In this self-consistent approach, we renormalize only the viscosity.

Following Wilson [15], we coarse-grain the system over a wave number shell, and compute the consequent correction to the viscosity. The wave number space is already divided in the shell model of turbulence, which makes the computation simpler than that for Navier-Stokes equation. The locality of interactions too simplifies the RG calculation. We denote the renormalized viscosity at wave number k_n by v_n .

Renormalization is often performed in (\mathbf{k}, ω) space. However, for the shell model, the renormalization calculation in (\mathbf{k}, t) space is concise and convenient. Hence, we adopt this scheme. In Appendix B, we will briefly discuss the renormalization of the shell model in (\mathbf{k}, ω) space.

For computing the renormalized viscosity at k_n in the inertial range where $f_n = 0$, we coarse grain the system by averaging over $u_{n+1}^{*>}(t)$ and $u_{n+2}^{>}(t)$ (see Fig. 1). Following RG convention, we label the variables to be averaged using the $>$ symbol, whereas those to be retained using the $<$ symbol.

Under this notation,

$$\left(\frac{d}{dt} + \bar{\nu}k_n^2\right)u_n^{<}(t) = -i[a_1 k_n u_{n+1}^{*>}(t)u_{n+2}^{>}(t) + a_2 k_{n-1} u_{n-1}^{*>}(t)u_{n+1}^{>}(t) - a_3 k_{n-2} u_{n-1}^{<}(t)u_{n-2}^{<}(t)]. \quad (2)$$

The variables with the $<$ superscript remain unaltered under coarse graining. However, $u_{n+1}^{>}(t)$ and $u_{n+2}^{>}(t)$ variables are assumed to be random with zero mean. Note that $u^>$ variables need not be Gaussian. Under these assumptions,

$$\langle u_{n-1}^{*<}(t)u_{n+1}^{>}(t) \rangle = u_{n-1}^{*<}(t)\langle u_{n+1}^{>}(t) \rangle = 0, \quad (3)$$

$$\langle u_{n-2}^{<}(t)u_{n-1}^{<}(t) \rangle = u_{n-2}^{<}(t)u_{n-1}^{<}(t). \quad (4)$$

Based on the above simplification,

$$\left(\frac{d}{dt} + \bar{\nu}k_n^2\right)u_n^{<}(t) - [ia_3 k_{n-2} u_{n-1}^{<}(t)u_{n-2}^{<}(t)] = -ia_1 k_n \langle u_{n+1}^{*>}(t)u_{n+2}^{>}(t) \rangle. \quad (5)$$

To compute the right-hand side (RHS) of Eq. (5), we evaluate $u_{n+1}^{*>}(t)$ and $u_{n+2}^{>}(t)$ using the Green's function technique. For example,

$$u_{n+2}^{>}(t) = \int_0^t dt' G_{n+2}(t-t')(-i)[a_1 k_n u_{n+3}^{*>}(t')u_{n+4}^{>}(t') + a_2 k_{n-1} u_{n+1}^{*>}(t')u_{n+3}^{>}(t') - a_3 k_n u_n^{<}(t')u_{n+1}^{>}(t')], \quad (6)$$

where $G_{n+2}(t-t')$ is the Green's function. Note, however, that $u_{n+3}^{*>}(t')$ and $u_{n+4}^{>}(t')$ are absent at this stage. Hence,

$$u_{n+2}^{>}(t) = \int_0^t dt' G_{n+2}(t-t')ia_3 k_n u_n^{<}(t')u_{n+1}^{>}(t'). \quad (7)$$

Substitution of Eq. (7) in the RHS of Eq. (5) yields

$$I_1 = \int_0^t dt' G_{n+2}(t-t')a_1 a_3 k_n^2 u_n^{<}(t')\langle u_{n+1}^{*>}(t)u_{n+1}^{>}(t') \rangle = a_1 a_3 k_n^2 \int_0^t dt' G_{n+2}(t-t')\bar{C}_{n+1}(t-t')u_n^{<}(t'), \quad (8)$$

where $\bar{C}_{n+1}(t-t')$ is the unequal time correlation.

In the self-consistent RG procedure, it is assumed that the decay rates of Green's and correlation functions are determined by the renormalized viscosity [9,24]. Hence,

$$G_n(t-t') = \theta(t-t') \exp[-v_n k_n^2 (t-t')], \quad (9)$$

$$\bar{C}_n(t-t') = C_n(t) \exp[-v_n k_n^2 (t-t')], \quad (10)$$

where $C_n(t)$ is the equal-time correlation ($t = t'$), and $\theta(t-t')$ is the step function, which is 0 for $t < t'$ and 1 for $t > t'$. Note that $G_n(\tau)$ and $\bar{C}_n(\tau)$ decay with a timescale of $\tau_c = (v_n k_n^2)^{-1}$. Equations (9) and (10) are valid for $\tau < \tau_c$ after which C_n and G_n decay rapidly to zero [1,28,29,29,39,40].

Substitution of $G_n(t-t')$ and $\bar{C}_n(t-t')$ of Eqs. (9) and (10) in Eq. (8) yields

$$I_1 = a_1 a_3 k_n^2 C_{n+1}(t) \int_0^t dt' \exp[-(v_{n+1} k_{n+1}^2 + v_{n+2} k_{n+1}^2)(t-t')] u_n^{<}(t'), \quad (11)$$

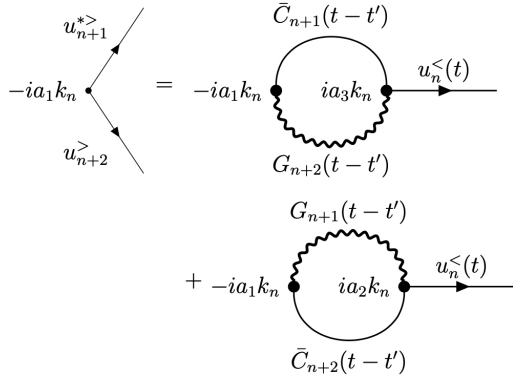


FIG. 2. Feynman diagrams associated with the viscosity renormalization. These diagrams are related to the RHS of Eq. (5).

Now, we employ the Markovian approximation, according to which the integral of Eq. (11) gets maximal contributions from t' near t [1]. This is possible when $\nu_n k_n^2 \gg 1$ [1]. Since the integral is peaked near $t = t'$, $u_n(t') \rightarrow u_n(t)$, and

$$I_1 = \frac{a_1 a_3 k_n^2 C_{n+1}(t)}{\nu_{n+1} k_{n+1}^2 + \nu_{n+2} k_{n+2}^2} u_n^{<}(t). \quad (12)$$

Such assumptions are made in Eddy-damped quasi-normal Markovian (EDQNM) approximation of hydrodynamic turbulence [1].

The RHS of Eq. (5) has another contribution to ν_n , which is computed by expanding $u_{n+1}^{* >}(t)$ using the Green's function. Following a similar approach as above, we compute the new term as

$$I_2 = \frac{a_1 a_2 k_n^2 C_{n+2}(t)}{\nu_{n+1} k_{n+1}^2 + \nu_{n+2} k_{n+2}^2} u_n^{<}(t). \quad (13)$$

The Feynman diagrams associated with I_1 and I_2 are exhibited in Fig. 2. Here, the loop diagrams represent the *self-energy* in which the wavy and solid lines are the Green's function and correlation function, respectively.

These calculations reveal that the RHS of Eq. (5) is proportional to $u_n^{<}$. Hence, the prefactors of I_1 and I_2 will provide corrections to $\bar{\nu}$ to yield ν_n . That is,

$$\nu_n k_n^2 = \bar{\nu} k_n^2 - \frac{a_1 k_n^2 [a_3 C_{n+1}(t) + a_2 C_{n+2}(t)]}{\nu_{n+1} k_{n+1}^2 + \nu_{n+2} k_{n+2}^2}. \quad (14)$$

Note, however, that $\bar{\nu} \ll \nu_n$. Hence,

$$\nu_n k_n^2 = - \frac{a_1 k_n^2 [a_3 C_{n+1}(t) + a_2 C_{n+2}(t)]}{\nu_{n+1} k_{n+1}^2 + \nu_{n+2} k_{n+2}^2}. \quad (15)$$

Note that we compute renormalized viscosity at the corresponding coarse-graining step. At the present level, $\nu_{n+1}, \nu_{n+2}, \dots$ have been computed already, whereas, $\nu_{n-1}, \nu_{n-2}, \dots$ would be computed at subsequent stages. Also note that during the computation of ν_{n-1} , $u_n^{>}$, and $u_{n+1}^{>}$ would belong to $>$ shells.

In Eq. (15), ν_n and C_n are both unknowns. RG equation for the Navier-Stokes equation too has a similar implicit form. Zhou *et al.* [38], and McComb and Shanmugasundaram [6] employed the self-consistent procedure to solve such an implicit equation (also see Refs. [5,37,41]). Following these

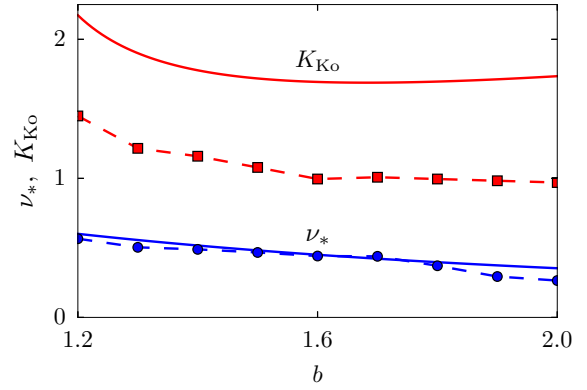


FIG. 3. For the shell model with various b 's, the RG constant ν_* computed using RG (solid blue curve) and using numerical simulations (blue circles). Also, K_{Ko} computed using field theory (solid red curve) and using numerical simulations (red squares). The analytical and numerical ν_* 's match quite well, but numerical K_{Ko} is around 1.6 times smaller than the analytical counterpart.

authors, we attempt the following functions for $C_n(t)$ and ν_n , which are inspired by Kolmogorov's theory of turbulence:

$$C_n(t) = K_{\text{Ko}} \epsilon^{2/3} k_n^{-2/3}, \quad (16)$$

$$\nu_n k_n^2 = \nu_* K_{\text{Ko}}^{1/2} \epsilon^{1/3} k_n^{2/3}, \quad (17)$$

where K_{Ko} is Kolmogorov's constant, ϵ is the viscous dissipation rate, and ν_* is the RG constant associated with ν_n . Substitution of the above in Eq. (15) yields

$$\nu_*^2 = - \frac{a_1 (a_3 b^{-2/3} + a_2 b^{-4/3})}{b^{2/3} + b^{4/3}}. \quad (18)$$

In Fig. 3, we plot ν_* for b ranging from 1.2 to 2.0. Here, $\nu_* \approx 0.5$, in particular, $\nu_* \approx 0.48$ for $b = 1.5$. The ν_* computed above are remarkably close to that for Navier-Stokes equation [5,6,37,38,41–43], which gives credence to the RG computation described in this paper.

It is important to note that the above derivation does not require quasi-Gaussian assumption for $u^>$ variables. We only need to assume time stationarity for these variables. In addition, we approximate $\langle u^< u^> \rangle = u^< \langle u^> \rangle = 0$ rather than expanding it further. These assumptions and local interactions in the shell model provide simplification in comparison to the RG calculations for the Navier-Stokes equation [5,6,37,38,41].

Equation (17) yields

$$\nu_{n+1}/\nu_n = (k_{n+1}/k_n)^{-4/3} = b^{-4/3}. \quad (19)$$

As is customary in quantum field theory [44], we make a change in variable as $b = \exp(l)$, with which

$$\nu_{n+1} = \nu_n \exp(-4l/3) \approx \nu_n [1 - 4l/3], \quad (20)$$

when $b \rightarrow 1$ or $l \rightarrow 0$. Hence,

$$\frac{d\nu}{dl} \approx -\frac{4}{3}\nu. \quad (21)$$

Therefore, ν_n increases with the decrease of k_n , akin to running coupling constant in quantum chromodynamics. Note, however, that ν_n is not the coupling constant; instead, it is the

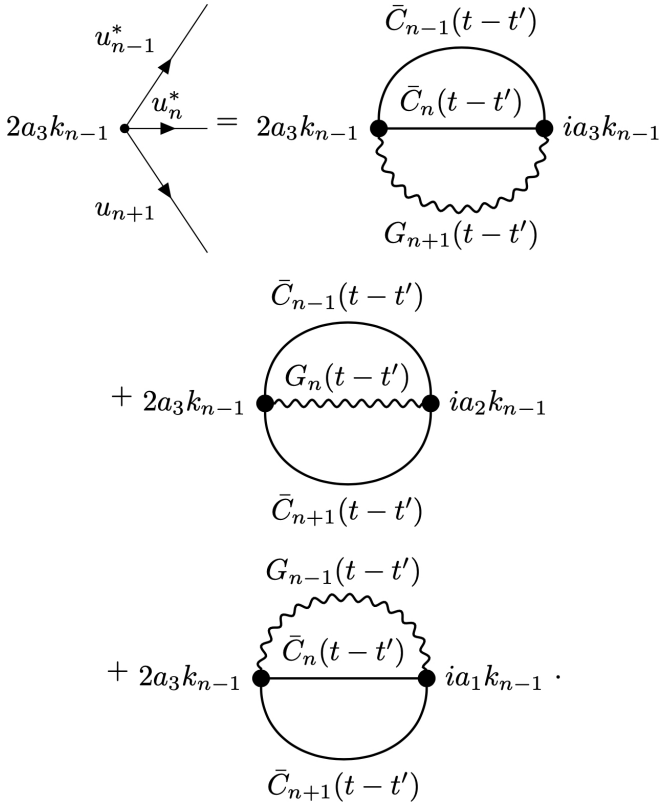


FIG. 4. Feynman diagrams associated with the first term of Eq. (23).

coefficient of the viscous term, which is linear (analogous to mass term in quantum field theory). We remark that the scaling of Eqs. (16), (17), and (21) breaks down when $k \rightarrow 1/L$, where L is the system size.

The dominant frequency at $k = k_n$ is

$$\omega_n \sim \nu_n k_n^2 \sim \epsilon^{1/3} k_n^{2/3}. \quad (22)$$

For small k_n , $\omega_n \rightarrow 0$. This is one of the assumptions of RG schemes in (\mathbf{k}, ω) space. Refer to Appendix B for details.

For $\bar{v} = 0$, $f_n = 0$, and the δ -correlated (white noise) initial condition, u_n remains δ correlated as in Euler turbulence [30,45,46]. Therefore, $\langle u_{n+1}^*(t) u_{n+2}^*(t) \rangle = 0$ [see Eq. (5)], leading to no correction or renormalization of the viscosity. Thus, $\nu_n = 0$ for the inviscid shell model. This solution corresponds to the *Gaussian fixed point* in Wilson's ϕ^4 theory [27].

In Sec. III, we will compute the energy flux for the shell model using field-theoretic techniques.

III. ENERGY FLUX COMPUTATION

In this section, we compute the energy flux for the shell model perturbatively. The energy flux at $k = k_n$ is defined as [33,35,47]

$$\begin{aligned} \Pi_n &= 2a_3 k_{n-1} \text{Im}[\langle u_{n-1}^*(t) u_n^*(t) u_{n+1}(t) \rangle] \\ &\quad - 2a_1 k_n \text{Im}[\langle u_n^*(t) u_{n+1}^*(t) u_{n+2}(t) \rangle]. \end{aligned} \quad (23)$$

We compute $\langle \Pi_n \rangle$ by averaging Eq. (23) under the assumption that $u_n(t)$'s in the inertial range are quasi-Gaussian with zero mean, an assumption used in the Eddy-Damped Quasi-

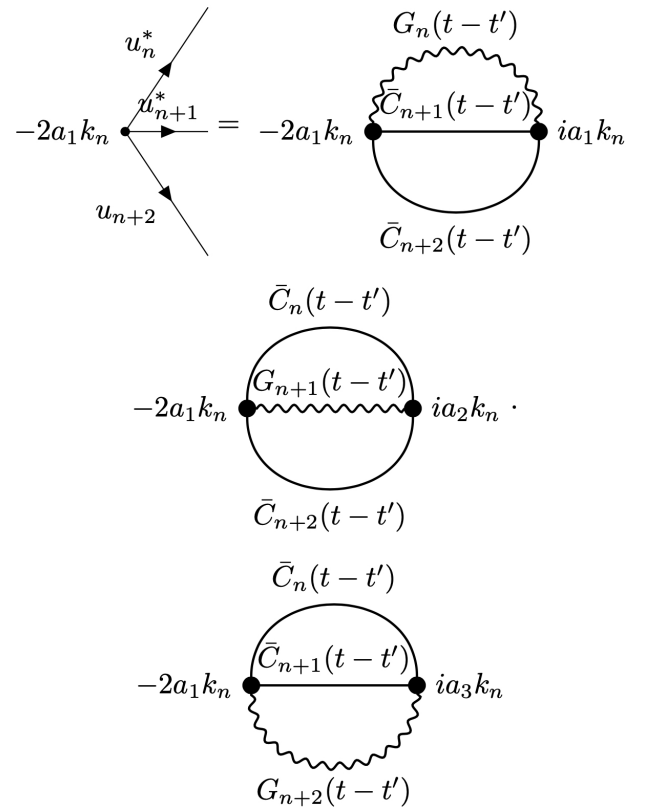


FIG. 5. Feynman diagrams associated with the second term of Eq. (23).

Normal Markovian (EDQNM) approximation and in Direct Interaction Approximation (DIA) [1,23]. To zeroth order, $\langle \Pi_n \rangle = 0$, which is the energy flux for Euler turbulence; this flux corresponds to the Gaussian fixed point $\nu = 0$.

However, $\langle \Pi_n \rangle \neq 0$ to the first order of perturbation. The Feynman diagrams associated with the first order in perturbation for the first and second terms of Eq. (23) are exhibited in Figs. 4 and 5, respectively. Let us analyze the expansion of the first Feynman diagram of Fig. 4. Here, $u_{n+1}(t)$ has been expanded as

$$\begin{aligned} u_{n+1}(t) &= \int_0^t dt' G_{n+1}(t-t') [-ia_1 k_{n+1} u_{n+2}^*(t') u_{n+3}(t') \\ &\quad - ia_2 k_n u_n^*(t') u_{n+2}(t') + ia_3 k_{n-1} u_n(t') u_{n-1}(t')], \end{aligned} \quad (24)$$

substitution of which in the first term of Eq. (23), or in the first Feynman diagram of Fig. 4, yields

$$\begin{aligned} I_3 &= 2a_3^2 k_{n-1}^2 \int_0^t dt' \exp[-\nu_{n+1} k_{n+1}^2 (t-t')] \\ &\quad \times \text{Im}[\langle i \langle u_n^*(t) u_{n-1}^*(t) u_n(t') u_{n-1}(t') \rangle \rangle] \\ &= 2a_3^2 k_{n-1}^2 \int_0^t dt' \exp[-\nu_{n+1} k_{n+1}^2 (t-t')] \\ &\quad \times \langle u_n^*(t) u_n(t') \rangle \langle u_{n-1}^*(t) u_{n-1}(t') \rangle \\ &= 2a_3^2 k_{n-1}^2 \frac{C_n C_{n-1}}{\nu_{n-1} k_{n-1}^2 + \nu_n k_n^2 + \nu_{n+1} k_{n+1}^2}. \end{aligned} \quad (25)$$

In the above derivation, we use the following properties:

$$(1) \langle u_n(t)u_m^*(t') \rangle = \delta_{n,m}C_n(t) \exp[-\nu_n k_n^2(t-t')].$$

(2) $\langle abcd \rangle = \langle ab \rangle \langle cd \rangle + \langle ac \rangle \langle bd \rangle + \langle ad \rangle \langle bc \rangle$ when $a, b, c,$ and d are Gaussian variables.

Using similar analysis, we derive the other integrals of the energy flux as

$$I_4 = 2a_2 a_3 k_{n-1}^2 C_{n-1} C_{n+1} / \text{denr1}, \quad (26)$$

$$I_5 = 2a_1 a_3 k_{n-1}^2 C_n C_{n+1} / \text{denr1}, \quad (27)$$

$$I_6 = -2a_1^2 k_n^2 C_{n+1} C_{n+2} / \text{denr2}, \quad (28)$$

$$I_7 = -2a_1 a_2 k_n^2 C_n C_{n+2} / \text{denr2}, \quad (29)$$

$$I_8 = -2a_1 a_3 k_n^2 C_n C_{n+1} / \text{denr2}, \quad (30)$$

with

$$\text{denr1} = \nu_{n-1} k_{n-1}^2 + \nu_n k_n^2 + \nu_{n+1} k_{n+1}^2, \quad (31)$$

$$\text{denr2} = \nu_n k_n^2 + \nu_{n+1} k_{n+1}^2 + \nu_{n+2} k_{n+2}^2. \quad (32)$$

The integrals $I_3, I_4,$ and I_5 correspond to the first term of Eq. (23), whereas $I_6, I_7,$ and I_8 correspond to the second term of Eq. (23). By adding I_3 to I_8 and using $k_n = k_0 b^n$, we derive

$$\langle \Pi_n \rangle = \epsilon = \frac{K_{\text{Ko}}^{3/2}}{\nu_*} \frac{\text{numr}}{1 + b^{2/3} + b^{4/3}}, \quad (33)$$

where

$$\begin{aligned} \text{numr} = & 2a_3 b^{-4/3} (a_1 b^{-2/3} + a_2 + a_3 b^{2/3}) \\ & - 2a_1 (a_1 b^{-2} + a_2 b^{-4/3} + a_3 b^{-2/3}). \end{aligned} \quad (34)$$

Equation (33) reveals that the energy flux is independent of wavenumber, consistent with Kolmogorov's theory of turbulence [48–50]. Using Eq. (33), we compute K_{Ko} and plot it in Fig. 3. We observe K_{Ko} to be a weak function of b . In particular, for $b = 1.5$, $K_{\text{Ko}} \approx 1.71$, which is close to the theoretical, experimental, and numerical values of Kolmogorov's constant [37,50].

IV. SWEEPING EFFECT IN THE SHELL MODEL

Kraichnan [30] showed that large-scale flow structures sweep smaller ones, a phenomenon called the *sweeping effect*. Here, large-scale velocity structures interact with small-scale ones. Kraichnan [30] observed that the sweeping effect leads to a $k^{-3/2}$ energy spectrum rather than the usual $k^{-5/3}$ spectrum. To overcome this discrepancy, Kraichnan [51] proposed the Lagrangian History Closure Approximation for turbulence. Note that the shell model involves local interactions, thus, drastically reduce the sweeping effect.

To test the sweeping effect in the field-theoretic calculation of the shell model, we introduce a term $iU_0 k_n u_n$ in the left-hand side of Eq. (1), where U_0 , a constant, represents the mean flow. Under renormalization, the above term appears as $iU_n k_n u_n^<$, where U_n represents the renormalized parameter corresponding to U_0 . With U_n , the RG flow equation [Eq. (15)] gets transformed to

$$iU_n k_n + \nu_n k_n^2 = -\frac{a_1 k_n^2 [a_3 C_{n+1} + a_2 C_{n+2}]}{\text{denr}}, \quad (35)$$

$$\text{denr} = i[U_{n+1} k_{n+1} + U_{n+2} k_{n+2}] + \nu_{n+1} k_{n+1}^2 + \nu_{n+2} k_{n+2}^2. \quad (36)$$

Using dimensional analysis, we argue that

$$U_n = U_* \epsilon^{1/3} k_n^{-1/3}, \quad (37)$$

substitution of Eqs. (16), (17), and (37) in Eq. (35) yields

$$(iU_* + \nu_*)^2 = -\frac{a_1 [a_3 b^{-2/3} + a_2 b^{-4/3}]}{b^{2/3} + b^{4/3}}. \quad (38)$$

The only possible solution of Eq. (38) is

$$U_* = 0, \quad \text{or} \quad U_n = 0, \quad (39)$$

and ν_* is given by the same formula as Eq. (18). Hence, the sweeping effect is absent in the RG calculation of the shell model, and $\nu(k)$ is independent of U_0 . However, in Sec. V, we show that the numerical results deviate from the above prediction.

V. NUMERICAL VERIFICATION

To test the predictions of the above field-theoretic calculations, we solve the Sabra shell model Eq. (1) numerically. We employ 40 shells, $\nu = 10^{-6}$, $U_0 = 0$, and fourth-order Runge-Kutta 4 time marching scheme with $dt = 10^{-5}$. The shell model is forced randomly at shells $n = 0$ and 1 so as to provide a constant energy supply rate; we choose $\epsilon = 2$ for all our runs. To test the dependence of ν and K_{Ko} on b , we vary b from 1.2 to 2 in the interval of 0.1. We also perform another simulation with $U_0 = 0.5$ and $b = 1.5$ to test the field-theoretic predictions on the sweeping effect. We carry out the simulations until 2000 eddy turnover times and report the energy spectra and fluxes after the system has reached a steady state.

As expected, for $U_0 = 0$ and finite ν , in the inertial range, the energy spectrum $C_n \sim k^{-2/3}$ and the energy flux $\Pi_n \approx \epsilon = 2$ [33,35,36]. See the red curves in Fig. 6 for an illustration for $b = 1.5$. Using Eq. (16), we compute the Kolmogorov's constants for various b 's and plot them in Fig. 3. We observe that for $b = 1.5$, $K_{\text{Ko}} = 1.05$, which is approximately 1.6 times smaller than the theoretically predicted value of 1.71 (for the shell model). See Fig. 3 for an illustration. This discrepancy between the numerical and the analytical K_{Ko} is possibly due to various approximations employed in the theoretical calculations, an issue that needs a closer investigation.

For the $U_0 = 0.5$ run, we again observe Kolmogorov's spectrum (apart from a hump) and constant energy flux (blue curves in Fig. 6). Here, $K_{\text{Ko}} \approx 0.92$. For the special case with $\bar{\nu} = 0$ and the white noise initial condition, numerical simulation yields $C_n \approx \text{constant}$ and nearly zero energy flux, consistent with the field-theoretic predictions. We illustrate the above energy spectrum and flux in the insets of Fig. 6.

To validate the renormalized viscosity of Eq. (17), we compute ν_n numerically using the normalized correlation function $R_n(\tau)$, which is defined as

$$R_n(\tau) = \frac{\bar{C}(\tau)}{C_n}, \quad (40)$$

where $\bar{C}(\tau)$ and C_n are the unequal-time and equal-time correlations, respectively [see Eq. (10)].

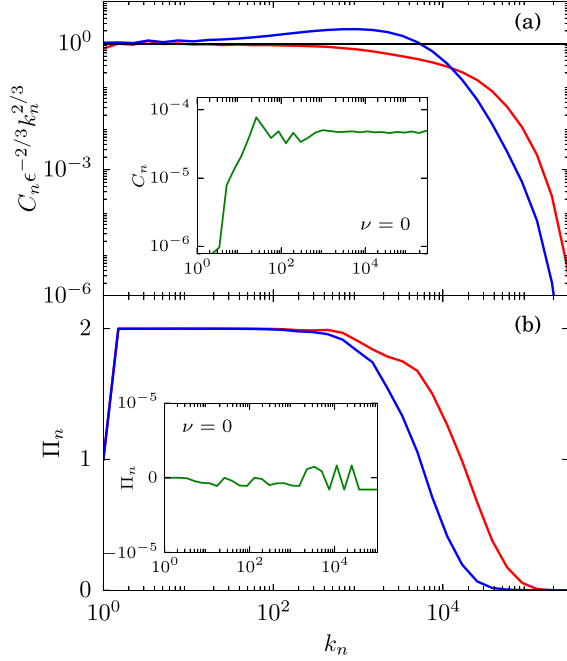


FIG. 6. For the numerical simulation of the shell model with $b = 1.5$: (a) plots of normalized energy spectra $C_n \epsilon^{-2/3} k_n^{2/3}$ vs k_n for $U_0 = 0$ (red curve) and $U_0 = 0.5$ (blue curve). (b) The corresponding energy fluxes Π_n are shown using the same color convention. We observe $C_n \sim k_n^{-2/3}$ and constant Π_n in the inertial range. The insets in (a) and (b) exhibit C_n and Π_n for the $\nu = 0$ case (equilibrium behavior).

We observe that the numerically computed $R_n(\tau)$ is real. For small τ and inertial range k_n 's, $R_n(\tau) \approx \exp[-k_n^{2/3} \tau]$, which is consistent with Eqs. (10) and (17). As illustrated in Fig. 7, for $b = 1.5$ and $U_0 = 0$,

$$R_n(\tau) \approx 1.03 \exp(-0.57 k_n^{2/3} \tau), \quad (41)$$

when $\nu_n k_n^2 \tau \lesssim 1$. A comparison of Eq. (41) with Eq. (10) reveals that $\nu_* \approx 0.57 / (K_{\text{Ko}}^{1/2} \epsilon^{1/3}) \approx 0.44$, which is in good agreement with the RG prediction of 0.48 (see Sec. II).

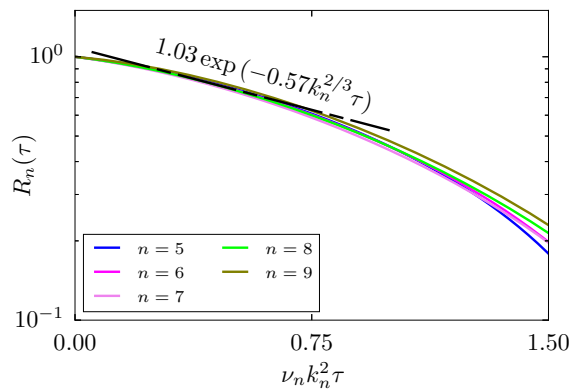


FIG. 7. For the shell-model simulation with $b = 1.5$ and $U_0 = 0$, plots of $R_n(\tau)$ vs $\nu_n k_n^2 \tau$ [Eq. (10)]. The chained straight line represents the best-fit curve $R_n(\tau) = 1.03 \exp(-0.57 k_n^{2/3} \tau)$ in the interval $\nu_n k_n^2 \tau = (0.1, 0.75)$.

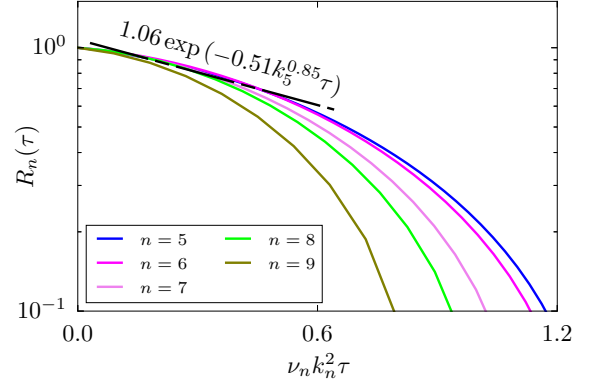


FIG. 8. For the shell-model simulation with $b = 1.5$ and $U_0 = 0.5$, plots of $R_n(\tau)$ vs $\nu_n k_n^2 \tau$. The chained straight line represents the best-fit curve $R_n(\tau) = 1.06 \exp(-0.51 k_n^{0.85} \tau)$ in the interval $\nu_n k_n^2 \tau = (0.1, 0.6)$ for $n = 5$. Note that the shells 8 and 9 do not follow the best-fit curve.

However, we cautiously remark that the numerical ν_* has significant errors.

For $U_0 = 0.5$, we compute $R_n(\tau)$ and fit it with $\exp(-\nu_n k_n^2 \tau)$. In Fig. 8, we plot $R_n(\tau)$ for shells $n = 5$ to 9. We observe that $R_n(\tau)$ for $U_0 = 0.5$ is steeper than the RG predictions. This is contrary to the RG prediction that the mean flow does not affect the renormalized viscosity. Clearly, the analytical computation underestimates the dissipation arising due to nonzero U_0 . This issue needs a closer examination that will be pursued in the future.

In Sec. VI, we compare our results with earlier RG works on the shell model and hydrodynamic turbulence.

VI. COMPARISON WITH EARLIER WORKS

There are only a small number of works on renormalization-group analysis of the shell model. Recently, Fontaine *et al.* [18] performed FRG analysis of the shell model and computed the multiscaling exponents. They observed that

$$C_n \sim k_n^{-\alpha_E}, \quad (42)$$

$$\nu_n k_n^2 \sim k_n^{\alpha_\nu}, \quad (43)$$

with $\alpha_E = 0.633 \pm .004$ and $\alpha_\nu = -0.741 \pm 0.01$. Substitution of the above in renormalization group equation [Eq. (15)] yields

$$\alpha_E + 2\alpha_\nu = 2. \quad (44)$$

Note that Fontaine *et al.* [18]'s α_E and α_ν satisfy Eq. (44) to a good approximation. Fontaine *et al.* [18] reported that the proportionality constant for $C_2(\tau = 0)$, which is K_{Ko} , is approximately 1.15.

In a different application of field theory, Eyink [10] employed operator product expansion to the shell model and computed various correlations and structure functions. Note, however, that Fontaine *et al.* [18] and Eyink [10] do not report the RG constant ν_* in their calculation. We remark that

the multiscaling exponents are related to the fluctuations in the energy flux, i.e., for $\langle \Pi_n^2 \rangle$ [42,52,53]. The self-consistent calculation presented in this paper may be extendible to the computation of $\langle \Pi_n^2 \rangle$.

It is important to compare our predictions on ν_* and K_{K_0} with the past works on hydrodynamic turbulence. Yakhot and Orszag [3] observed that $\nu_* = 0.39$ and $K_{K_0} = 1.617$. McComb and Shanmugasundaram [7] computed that $\nu_* \approx 0.40$ and $K_{K_0} \approx 1.8$. Zhou *et al.* [38] also reported $\nu_* \approx 0.40$. Our field-theoretic computation of the shell model yields $\nu_* \approx 0.50$ and $K_{K_0} = 1.7$, with minor variations depending on the value of b . Using ERG, Tomassini [17] showed that $E(k) \sim k^{-1.666 \pm 0.001}$, whereas K_{K_0} lies in the range of 1.124 to 1.785 depending on the chosen function. Clearly, the shell-model predictions are reasonably close to the earlier works on hydrodynamic turbulence.

There are subtle differences between the RG schemes for the shell model and hydrodynamic turbulence. The RG procedure for the shell model does not involve any integral and, hence, is simpler than that for hydrodynamic turbulence. In addition, we make fewer assumptions in the RG implementation of the shell model. For example, $u^>$ variables are assumed to be time-stationary but not necessarily quasi-Gaussian. Note that many past RG works assume that $u^>$ is quasi-Gaussian (see e.g., Ref. [9]). In addition, the RG computation of the shell model is nearly exact. In Eq. (5), we substitute the expansion of $u_{n+1}^{*>}$ and $u_{n+2}^{>}$ one after the other, and then solve for the ν_n under Markovian approximation. Also, note that the local interactions in the shell model suppresses the *sweeping effect* proposed by Kraichnan [30].

We conclude in the next section.

VII. CONCLUSIONS

In this paper, we employ RG analysis to the shell model of turbulence and show that a combination of Kolmogorov's spectrum $C_n = K_{K_0} \epsilon^{2/3} k_n^{-2/3}$ and $\nu_n = \nu_* K_{K_0}^{1/2} \epsilon^{1/3} k_n^{-4/3}$ is a solution of the RG flow equation. Our calculations predict that for $b = 1.5$, $\nu_* \approx 0.48$, and $K_{K_0} \approx 1.71$, which are in good agreement with the numerical results, except that the numerical K_{K_0} is around 1.6 times smaller than the theoretical prediction. Note that the field-theoretic predictions for the shell model and the Navier-Stokes equation are close to each other [6,37,38].

The computation employed in this paper can be easily generalized to the shell models for scalar and magnetohydrodynamic turbulences. We also believe that the fluctuations in the energy flux for the shell model could be computed using the method outlined in this paper.

ACKNOWLEDGMENTS

We thank anonymous referees for useful comments and suggestions. We also thank Soumyadeep Chatterjee for helping us in making Feynman diagrams. This work is supported by Project No. 6104-1 from the Indo-French Centre for the Promotion of Advanced Research (IFPAR/CEFIPRA), and Project No. PHY/DST/2020455 by the Department of Science and Technology, India.

APPENDIX A: GALILEAN INVARIANCE LEADS TO NONRENORMALIZABILITY OF THE COUPLING CONSTANT

It can be easily shown that the coupling constant λ of NSE remain unchanged on renormalization due to Galilean invariance [2,9,37]. Here, the derivation is reproduced in brief.

We write the renormalized Navier-Stokes equation as

$$\partial_t \mathbf{u}(\mathbf{x}, t) + \lambda \mathbf{u}(\mathbf{x}, t) \cdot \nabla \mathbf{u}(\mathbf{x}, t) = -\nabla p(\mathbf{x}, t) + \nu \nabla^2 \mathbf{u}(\mathbf{x}, t), \quad (\text{A1})$$

where $\mathbf{u}(\mathbf{x}, t)$ and $p(\mathbf{x}, t)$ are the velocity and pressure fields, respectively, λ is a measure of the nonlinear interaction, and ν is the kinematic viscosity. Note that $\lambda = 1$ for the original NSE, but it may get renormalized under scaling.

We consider two reference frames: *laboratory references frame*, where the fluid has mean velocity $\mathbf{U}_0 = U_0 \hat{x}$, and the *moving reference frame*, where the velocity is $\mathbf{u}'(\mathbf{x}', t')$ with zero mean. We denote the variables in the laboratory frames using unprimed variables, but those in the moving frame using primed variables. The variables in the two reference frames are related to each other via Galilean transformation, which is

$$x = x' + U_0 t', \quad y = y', \quad z = z', \quad t = t'; \quad (\text{A2})$$

$$\partial_x = \partial_{x'}, \quad \partial_y = \partial_{y'}, \quad \partial_z = \partial_{z'}, \quad \partial_t = \partial_{t'} - U_0 \partial_{x'}; \quad (\text{A3})$$

$$\mathbf{u}(\mathbf{x}, t) = U_0 \hat{x} + \mathbf{u}'(\mathbf{x}', t'), \quad p(\mathbf{x}, t) = p'(\mathbf{x}', t'), \quad (\text{A4})$$

substitution of which in Eq. (A1) yields

$$\begin{aligned} \partial_{t'} \mathbf{u}'(\mathbf{x}', t') + \lambda [U_0 \hat{x} + \mathbf{u}'(\mathbf{x}', t')] \nabla' \mathbf{u}'(\mathbf{x}', t') - U_0 \partial_{x'} \mathbf{u}'(\mathbf{x}', t') \\ = -\nabla' p'(\mathbf{x}, t) + \nu \nabla'^2 \mathbf{u}'(\mathbf{x}', t'). \end{aligned} \quad (\text{A5})$$

Note that Eq. (A5) is transformed to Eq. (A1) in primed variables only if

$$\lambda = 1. \quad (\text{A6})$$

Thus, it has been shown that λ is unchanged under RG due to Galilean invariance. For further discussion, refer to Forster *et al.* [2] and McComb [37,9].

The shell model is written in Fourier space. Hence, it is not possible to extend the above derivation to the shell model. However, using the analogy between the shell model and the Navier-Stokes equation, it is reasonable to assume that $\lambda = 1$ for the shell model and that λ remains unaltered under RG operation.

APPENDIX B: RENORMALIZATION OF THE SHELL MODEL IN (\mathbf{k}, ω) SPACE

In this Appendix, we will briefly discuss renormalization of the shell model in (\mathbf{k}, ω) space. Note that the shell model is already divided in \mathbf{k} space. The forward and inverse Fourier transforms of u_n are defined as follows:

$$u_n(t) = \int_{-\infty}^{\infty} \frac{d\omega}{2\pi} u_n(\omega) \exp[-i\omega t], \quad (\text{B1})$$

$$u_n(\omega) = \int_{-\infty}^{\infty} dt u_n(t) \exp[i\omega t]. \quad (\text{B2})$$

Fourier transform of Eq. (1) yields the following equation for $u_n^<(\omega)$:

$$\begin{aligned} (-i\omega + \bar{\nu}k_n^2)u_n^<(\omega) = & -i \int \frac{d\omega'}{2\pi} [a_1 k_n u_{n+1}^{*>}(\omega' - \omega) u_{n+2}^>(\omega') \\ & + a_2 k_{n-1} u_{n-1}^{*<}(\omega' - \omega) u_{n+1}^>(\omega') \\ & - a_3 k_{n-2} u_{n-2}^<(\omega - \omega') u_{n-1}^<(\omega')]. \end{aligned} \quad (\text{B3})$$

We perform ensemble averaging over $u_{n+1}^>$ and $u_{n+2}^>$ variables. Following the method of Sec. II, we arrive at

$$\langle u_{n-1}^{*<}(\omega' - \omega) u_{n+1}^>(\omega') \rangle = 0, \quad (\text{B4})$$

$$\langle u_{n-2}^<(\omega - \omega') u_{n-1}^<(\omega') \rangle = u_{n-2}^<(\omega - \omega') u_{n-1}^<(\omega'). \quad (\text{B5})$$

Consequently, only the first term of Eq. (B3) yields a nonzero correction to the viscosity.

The renormalized viscosity receives contributions from the two Feynman diagrams of Fig. 2. For the first loop diagram, we expand $u_{n+2}^>(\omega')$ as follows:

$$\begin{aligned} (-i\omega' + \nu_{n+2}k_{n+2}^2)u_{n+2}^>(\omega') \\ = -i \int \frac{d\omega''}{2\pi} [a_1 k_{n+2} u_{n+3}^{*>}(\omega'' - \omega') u_{n+4}^>(\omega'') \\ + a_2 k_{n+1} a_2 u_{n+1}^{*>}(\omega'' - \omega') u_{n+3}^>(\omega'') \\ - a_3 k_n u_n^<(\omega' - \omega'') u_{n+1}^>(\omega'')]. \end{aligned} \quad (\text{B6})$$

Note, however, that $u_{n+3}^{*>}(\omega)$ and $u_{n+4}^{*>}(\omega)$ are absent at this stage of expansion. Hence, only the last term of Eq. (B6) survives. Therefore,

$$u_{n+2}^>(\omega') = ia_3 k_n \int \frac{d\omega''}{2\pi} \frac{u_n^<(\omega' - \omega'') u_{n+1}^>(\omega'')}{-i\omega' + \nu_{n+2}k_{n+2}^2}, \quad (\text{B7})$$

substitution of which in the RHS of Eq. (B3) yields

$$\begin{aligned} X = & -ia_1 k_n \int \frac{d\omega'}{2\pi} \langle u_{n+1}^{*>}(\omega' - \omega) u_{n+2}^>(\omega') \rangle \\ = & a_1 a_3 k_n^2 \int \frac{d\omega'}{2\pi} \frac{d\omega''}{2\pi} \frac{\langle u_{n+1}^{*>}(\omega' - \omega) u_{n+1}^>(\omega'') \rangle}{-i\omega' + \nu_{n+2}k_{n+2}^2} \\ & \times u_n^<(\omega' - \omega''), \\ = & \left[a_1 a_3 k_n^2 \int \frac{d\omega'}{2\pi} \frac{\langle |u_{n+1}^>(\omega' - \omega)|^2 \rangle}{-i\omega' + \nu_{n+2}k_{n+2}^2} \right] u_n^<(\omega). \end{aligned} \quad (\text{B8})$$

Since ν_n is computed for a long time limit, we set $\omega \rightarrow 0$ in the above integral. Hence, the square-bracketed term of Eq. (B8) is

$$I_1 = a_1 a_3 k_n^2 \int \frac{d\omega'}{2\pi} \frac{\langle |u_{n+1}^>(\omega')|^2 \rangle}{-i\omega' + \nu_{n+2}k_{n+2}^2}. \quad (\text{B9})$$

Now, we employ Wiener-Khinchin theorem to simplify the frequency spectrum as

$$\langle |u_{n+1}^>(\omega')|^2 \rangle = \int_{-\infty}^{\infty} d\tau C_{n+1}(\tau) \exp(-i\omega'\tau), \quad (\text{B10})$$

where $C_{n+1}(\tau)$ is the correlation function defined in Eq. (10). With this,

$$I_1 = a_1 a_3 k_n^2 \int_{-\infty}^{\infty} d\tau \bar{C}_{n+1}(\tau) \int \frac{d\omega'}{2\pi} \frac{\exp(-i\omega'\tau)}{-i\omega' + \nu_{n+2}k_{n+2}^2}. \quad (\text{B11})$$

An application of contour integral over the lower part of ω' plane yields

$$\begin{aligned} I_1 = & a_1 a_3 k_n^2 C_{n+1} \int_0^{\infty} d\tau \exp[-(\nu_{n+1}k_{n+1}^2 + \nu_{n+2}k_{n+2}^2)\tau] \\ = & \frac{a_1 a_3 k_n^2 C_{n+1}}{\nu_{n+1}k_{n+1}^2 + \nu_{n+2}k_{n+2}^2}. \end{aligned} \quad (\text{B12})$$

The second Feynman diagram of Fig. 2 yields

$$I_2 = \frac{a_1 a_2 k_n^2 C_{n+2}}{\nu_{n+1}k_{n+1}^2 + \nu_{n+2}k_{n+2}^2}. \quad (\text{B13})$$

The steps beyond this point are same as those described in Sec. II.

-
- [1] S. A. Orszag, in *Les Houches Summer School of Theoretical Physics*, edited by R. Balian and J. L. Peube (North-Holland, Amsterdam, 1973), p. 235.
- [2] D. Forster, D. R. Nelson, and M. J. Stephen, *Phys. Rev. A* **16**, 732 (1977).
- [3] V. Yakhot and S. A. Orszag, *J. Sci. Comput.* **1**, 3 (1986).
- [4] Y. Zhou, G. Vahala, and M. Hossain, *Phys. Rev. A* **40**, 5865 (1989).
- [5] Y. Zhou, *Phys. Rep.* **488**, 1 (2010).
- [6] W. D. McComb and V. Shanmugasundaram, *Phys. Rev. A* **28**, 2588 (1983).
- [7] W. D. McComb and V. Shanmugasundaram, *J. Phys. A: Math. Gen.* **18**, 2191 (1985).
- [8] W. D. McComb, *Renormalization Methods: A Guide for Beginners* (Oxford University Press, Oxford, 2004).
- [9] W. D. McComb, *Homogeneous, Isotropic Turbulence: Phenomenology, Renormalization and Statistical Closures* (Oxford University Press, Oxford, 2014).
- [10] G. L. Eyink, *Phys. Rev. E* **48**, 1823 (1993).
- [11] P. C. Martin, E. D. Siggia, and H. A. Rose, *Phys. Rev. A* **8**, 423 (1973).
- [12] J. K. Bhattacharjee, *Phys. Fluids A* **3**, 879 (1991).
- [13] L. T. Adzhemyan, N. V. Antonov, and A. N. Vasiliev, *Field Theoretic Renormalization Group in Fully Developed Turbulence* (CRC Press, Boca Raton, FL, 1999).
- [14] K. G. Wilson, *Phys. Rev. D* **3**, 1818 (1971).

- [15] K. G. Wilson, *Rev. Mod. Phys.* **55**, 583 (1983).
- [16] J. Polchinski, *Nucl. Phys. B* **231**, 269 (1984).
- [17] P. Tomassini, *Phys. Lett. B* **411**, 117 (1997).
- [18] C. Fontaine, M. Tarpin, F. Bouchet, and L. Canet, [arXiv:2208.00225](https://arxiv.org/abs/2208.00225).
- [19] L. Canet, *J. Fluid Mech.* **950**, P1 (2022).
- [20] A. A. Fedorenko, P. L. Doussal, and K. J. Wiese, *J. Stat. Mech.* (2013) P04014.
- [21] C. Mejía-Monasterio and P. Muratore-Ginanneschi, *Phys. Rev. E* **86**, 016315 (2012).
- [22] L. Biferale, A. A. Mailybaev, and G. Parisi, *Phys. Rev. E* **95**, 043108 (2017).
- [23] R. H. Kraichnan, *J. Fluid Mech.* **5**, 497 (1959).
- [24] D. C. Leslie, *Developments in the Theory of Turbulence* (Clarendon Press, Oxford, 1973).
- [25] A. L. Fairhall, B. Dhruva, V. S. L'vov, I. Procaccia, and K. R. Sreenivasan, *Phys. Rev. Lett.* **79**, 3174 (1997).
- [26] G. Falkovich, K. Gawędzki, and M. Vergassola, *Rev. Mod. Phys.* **73**, 913 (2001).
- [27] K. G. Wilson and J. Kogut, *Phys. Rep.* **12**, 75 (1974).
- [28] T. Sanada and V. Shanmugasundaram, *Phys. Fluids* **4**, 1245 (1992).
- [29] M. K. Verma, A. Kumar, and A. Gupta, *Trans Indian Natl. Acad. Eng.* **5**, 649 (2020).
- [30] R. H. Kraichnan, *Phys. Fluids* **7**, 1723 (1964).
- [31] V. S. L'vov, E. Podivilov, A. Pomyalov, I. Procaccia, and D. Vandembroucq, *Phys. Rev. E* **58**, 1811 (1998).
- [32] V. S. L'vov, E. Podivilov, and I. Procaccia, *Europhys. Lett.* **46**, 609 (1999).
- [33] L. Biferale, *Annu. Rev. Fluid Mech.* **35**, 441 (2003).
- [34] P. Constantin, B. Levant, and E. S. Titi, *Physica D* **219**, 120 (2006).
- [35] P. D. Ditlevsen, *Turbulence and Shell Models* (Cambridge University Press, Cambridge, UK, 2010).
- [36] F. Plunian, R. Stepanov, and P. Frick, *Phys. Rep.* **523**, 1 (2013).
- [37] W. D. McComb, *The Physics of Fluid Turbulence* (Clarendon Press, Oxford, 1990).
- [38] Y. Zhou, G. Vahala, and M. Hossain, *Phys. Rev. A* **37**, 2590 (1988).
- [39] S. B. Pope, *Turbulent Flows* (Cambridge University Press, Cambridge, UK, 2000).
- [40] Y. Zhou, *Phys. Rep.* **935**, 1 (2021).
- [41] Y. Zhou, *Phys. Fluids A* **5**, 1092 (1993).
- [42] M. K. Verma, [arXiv:nlin/0510069](https://arxiv.org/abs/nlin/0510069).
- [43] M. K. Verma, *Phys. Rep.* **401**, 229 (2004).
- [44] M. E. Peskin and D. V. Schroeder, *An Introduction To Quantum Field Theory* (The Perseus Books Group, Reading, MA, 1995).
- [45] M. K. Verma, S. Bhattacharya, and S. Chatterjee, [arXiv:2004.09053](https://arxiv.org/abs/2004.09053).
- [46] M. K. Verma and S. Chatterjee, *Phys. Rev. Fluids* **7**, 114608 (2022).
- [47] M. K. Verma, *Energy Transfers in Fluid Flows: Multiscale and Spectral Perspectives* (Cambridge University Press, Cambridge, UK, 2019).
- [48] A. N. Kolmogorov, *Dokl Acad Nauk SSSR* **32**, 16 (1941).
- [49] A. N. Kolmogorov, *Dokl Acad Nauk SSSR* **30**, 301 (1941).
- [50] U. Frisch, *Turbulence: The Legacy of A. N. Kolmogorov* (Cambridge University Press, Cambridge, UK, 1995).
- [51] R. H. Kraichnan, *Phys. Fluids* **8**, 575 (1965).
- [52] K. R. Sreenivasan, *Annu. Rev. Fluid Mech.* **23**, 539 (1991).
- [53] A. Das and J. K. Bhattacharjee, *Europhys. Lett.* **26**, 527 (1994).